

Adult Mesenchymal Stem Cells and Derivatives in Improved Elastin Homeostasis in a Rat Model of Abdominal Aortic Aneurysms

Shataakshi Dahal¹, Simran Dayal¹, Charlie Androjna², John Peterson³, Anand Ramamurthi^{*1} 

¹Lehigh University, Department of Bioengineering, Bethlehem, PA, USA

²Cleveland Clinic, Lerner Research Institute, Department of Biomedical Engineering, Cleveland, OH, USA

³Cleveland Clinic, Lerner Research Institute, Department of Research Core Administration, Cleveland, OH, USA

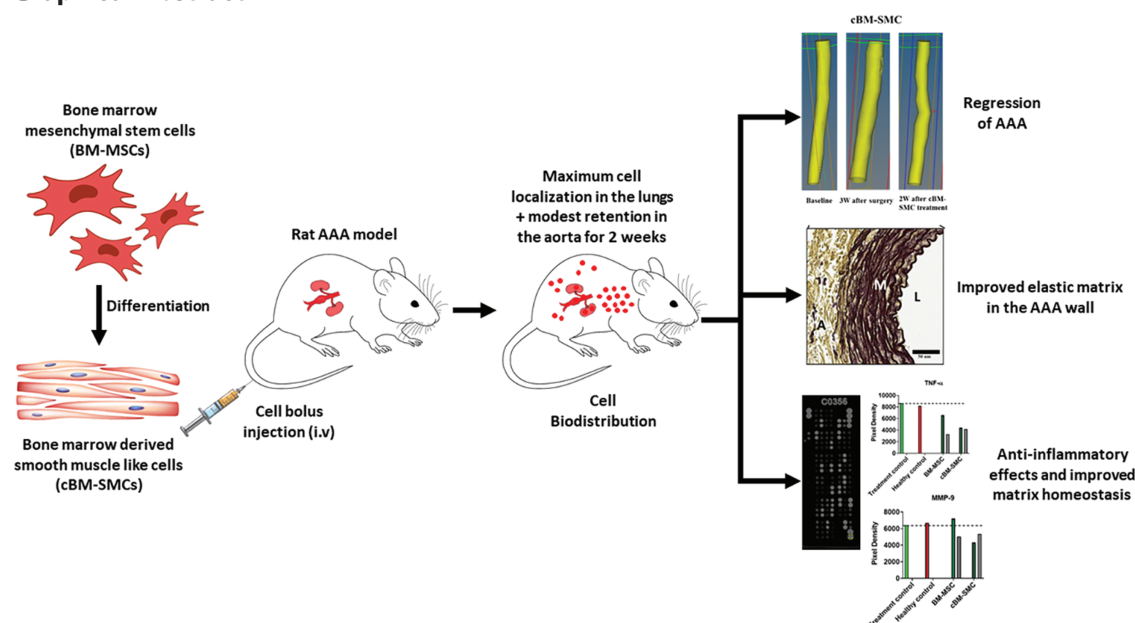
*Corresponding author: Anand Ramamurthi, 111 Research Drive, Iacocca Hall, D-325, Bethlehem, PA 18015, USA. Email: anr320@lehigh.edu

Abstract

Abdominal aortic aneurysms (AAAs) are localized rupture-prone expansions of the aorta with limited reversibility that develop due to proteolysis of the elastic matrix. Natural regenerative repair of an elastic matrix is difficult due to the intrinsically poor elastogenicity of adult vascular smooth muscle cells (VSMCs). This justifies the need to provide external, pro-elastin regenerative- and anti-proteolytic stimuli to VSMCs in the AAA wall towards reinstating matrix structure in the aorta wall. Introducing alternative phenotypes of highly elastogenic and contractile cells into the AAA wall capable of providing such cues, proffers attractive prospects for AAA treatment. In this regard, we have previously demonstrated the superior elastogenicity of bone marrow mesenchymal stem cell (BM-MSC)-derived SMCs (cBM-SMCs) and their ability to provide pro-elastogenic and anti-proteolytic stimuli to aneurysmal SMCs *in vitro*. However, the major issues associated with cell therapy, such as their natural ability to home into the AAA tissue, their *in vivo* biodistribution and retention in the AAA wall, and possible paracrine effects on AAA tissue repair processes in the event of localization in remote tissues remain uncertain. Therefore, in this study we focused on assessing the fate, safety, and AAA reparative effects of BM-MSC-derived cBM-SMCs *in vivo*. Our results indicate that the cBM-SMCs (a) possess natural homing abilities similar to the undifferentiated BM-MSCs, (b) exhibit higher retention upon localization in the aneurysmal aorta than BM-MSCs, (c) downregulate the expression of several inflammatory and pro-apoptotic cytokines that are upregulated in the AAA wall contributing to accelerated elastic matrix breakdown and suppression of elastic fiber neo-assembly, repair, and crosslinking, and (d) improve elastic matrix content and structure in the AAA wall toward slowing the growth of AAAs. Our study provides initial evidence of the *in vivo* elastic matrix reparative benefits of cBM-SMCs and their utility in cell therapy to reverse the pathophysiology of AAAs.

Key words: abdominal aortic aneurysms (AAAs); cell therapy; stem cells; extracellular matrix; elastin.

Graphical Abstract



Received: 26 October 2021; Accepted: 4 February 2022.

© The Author(s) 2022. Published by Oxford University Press.

This is an Open Access article distributed under the terms of the Creative Commons Attribution-NonCommercial License (<https://creativecommons.org/licenses/by-nc/4.0/>), which permits non-commercial re-use, distribution, and reproduction in any medium, provided the original work is properly cited. For commercial re-use, please contact journals.permissions@oup.com.

Significance Statement

The ability of bone marrow mesenchymal stem cell (BM-MSC)-derived smooth muscle cells (SMCs) (cBM-SMCs) to robustly synthesize elastic matrix, which adult vascular cells are incapable of achieving, and their unique ability, unlike undifferentiated BM-MSCs, to provide pro-elastogenic and anti-proteolytic stimuli to aneurysmal SMCs via their paracrine secretions, and yet maintain high contractile abilities of SMCs in healthy vessels, renders their use in abdominal aortic aneurysm cell therapy highly significant. While use of allogeneic BM-MSCs for cell therapy is acceptable even in the clinic, we expect our study of these cells to guide future investigation of patient-derived cells, which can potentially enable patient customized treatments.

Introduction

Adult stem cells are widely used in the study of cardiovascular diseases such as heart failure, myocardial infarction, and ischemic heart disease.^{1,2} Besides their purported ability to home into the tissue site of disease or injury,³ there is also evidence that these stem cells can initiate biological signaling cascades that can work through paracrine mechanisms to regenerate or heal tissues.^{4,6} In the context of cell therapy, there is evidence that MSCs are immune system-privileged and possess anti-inflammatory properties, which can reduce possible rejection when allo- or xeno-transplanted.^{2,7} Their pluripotency also enables their differentiation into cell types of multiple lineages, including vascular cells, with the prospects of regenerating, repairing, and restoring tissue function.⁴ Several studies have sought to investigate the differentiation of BM-MSCs into other cell types like bone cells or vascular smooth muscle cells in the context of ECM regeneration particularly collagen⁸ the elastic matrix regenerative potential of these stem cells and their vascular SMC-like derivatives are far less studied, particularly in the context of neo-assembly of elastic fibers, which are not naturally regenerated in adult tissues.

Abdominal aortic aneurysms (AAAs) are cardiovascular pathologies that involve breakdown and loss of aortal wall structural extracellular matrix (ECM) leading to gradual wall thinning, weakening, and ultimate rupture.⁹ More specifically, AAA pathophysiology involves (a) upregulation of proinflammatory cytokines, (b) chronic overexpression of proteolytic enzymes such as matrix metalloproteases (MMPs), (c) progressive breakdown and loss of elastic fibers, ECM components that enable vessel stretch and recoil, by MMPs-2 and 9, and (d) apoptosis of medial smooth muscle cells (SMCs), the primary cells that remodel the injured vessel wall.¹⁰ Restoring elastic matrix homeostasis in the AAA wall is critical to reversing AAA pathophysiology to restore a healthy vessel state but is a significant challenge in the absence of appropriate regenerative tools to accomplish this. This is impeded by the naturally poor and impaired ability of adult and diseased vascular cells to regenerate or repair wall elastic matrix. Based on studies strongly suggesting the involvement of stem cells (SCs) and SC-derived smooth muscle cells (SMCs) in vascular morphogenesis,¹¹⁻¹³ and tissue repair after injury,¹⁴ which are the only physiologic scenarios in the vasculature wherein elastic matrix is prolifically synthesized,^{15,16} in prior work, we showed successful differentiation of rat bone marrow mesenchymal stem cells (BM-MSCs) into SMC like cells of specific phenotypes (cBM-SMCs)¹⁵⁻¹⁷ that exhibited high elastogenicity, anti-proteolytic properties, and high contractility in vitro 2D and 3D culture models.¹⁵⁻¹⁷ While the cells retained their phenotype and superior elastogenicity in long-term culture,^{15,16} there are several unknowns associated with their physical delivery in vivo for cell therapy. These include their biodistribution in different organs following

intravenous infusion, their ability to home into the injured AAA wall and subsequent retention on-site, and possible paracrine effects on AAA wall repair processes even in the event of localizing in remote tissues. We thus now investigate the natural homing of cBM-SMCs to the AAA wall upon intravenous injection of a bolus of these cells in the rat AAA model, and their biodistribution in other organs. We also sought to generate initial evidence of their therapeutic potential for restoring elastin homeostasis and slowing or reversing AAA growth in vivo.

Materials and Methods

Experimental Design

The experimental design is shown in [Supplementary Fig. S1](#) and described in [Supplementary Methods 1](#).

Generating Small AAAs in Rat Model

All animal procedures were conducted with the approval of the Institutional Animal Care and Use Committee (IACUC) at the Cleveland Clinic (ARC # 2019-2107). The animal facility at Cleveland Clinic is AAALAC-approved (Animal Assurance # A3145-01). AAAs were induced in male Sprague Dawley rats (Young Adult, 150-210 g, Charles River Laboratory, Wilmington, MA, USA) using an elastase injury method previously published by our lab.¹⁸ The details have been described in [Supplementary Methods 2](#).

Characterizing AAA Size by Small Animal Magnetic Resonance Imaging (MRI)

AAA formation was confirmed and the effects of cell injection on AAA size were assessed by non-invasive characterization using a small animal MRI (BioSpec 70/20 7T, Bruker Biospin Corp., Billerica, MA). Scanning was performed just prior to surgery to measure the baseline aortal volume and also at 3 weeks post-surgery (ie, day of cell injection), 1 week after cell infusion, and 2 weeks after cell infusion to monitor aortal volume changes. For MRI, the rats were anesthetized with 2% v/v isoflurane as described above and positioned in a prone position in a BioSpec 70/20 Bruker MRI system with the abdominal region aligned at the center of the magnetic field of the MR coil. 3D Phase-contrast angiography (PCA), which scans moving fluid or blood without requiring the contrast agents, was used to visualize the aorta. Volumetric analysis of the scans was performed after imaging to obtain the volume changes in the abdominal aorta subjected to AAA induction or cell treatment after AAA formation. A 3-D rendering of the aorta was generated using the software Microview Parallax™ (Parallax Innovations, Ontario, Canada) by subtracting the background to isolate the aorta and vena cava. The aneurysmal segment of the aorta and the number of slices within

the segment were identified for the sequential scans of each animal to analyze the equal segment length for each animal. The volume was measured by tracing the contours of the circumference of the aortal segment in a transverse plane along the length of the aorta at every 5 slices between the clamped region from below the kidney (renal bifurcation) to just above the iliac bifurcation. The % change in volumes between the (a) aorta at baseline and the AAA segment pre-treatment and (b) the aorta at baseline and following treatment (1 or 2 weeks post cell infusion) was plotted. Two-way mixed model ANOVA was used to compare the statistical significance between the groups for each dose, and 2-way ANOVA was used to compare the effect of a number of dosing events and the effect of time between the groups and within the groups.

Labeling and Intravenous Injection of BM-SMCs and cBM-SMCs

Rat BM-MSCs (Cyagen, Santa Clara, CA, USA; passages 2–5) were propagated in culture as described in earlier published studies.¹⁵ Briefly, the cells were cultured at a density of $2 \times 10^3/\text{cm}^2$ in a T-75 flask supplemented with low glucose DMEM containing 10% v/v MSC-quantified FBS (Gibco, Gaithersburg, MD, USA) and 1% v/v PenStrep (ThermoFisher Scientific, Waltham, MA). At confluence, these cells were trypsinized and differentiated into cBM-SMCs. Briefly, BM-MSCs were cultured as described above at a density of 2×10^3 cells/ cm^2 in low-glucose DMEM. Upon attaining confluence, the cells were re-seeded onto human fibronectin (hFN, 100 ng/mL)-coated tissue-culture flasks (BD Biosciences, East Rutherford, NJ, USA) at a density of 2×10^3 cells/ cm^2 and cultured in differentiation medium (DMEM low glucose, fetal bovine serum, dexamethasone, epidermal growth factor, insulin-transferrin selenium, leukemia inhibitory factor, linoleic acid albumin, MCDB 201, PenStrep, 2-phospho-L-ascorbic acid trisodium salt, PDGF and TGF- β).¹⁹ At 21 days into the differentiation process, the cells were trypsinized and seeded in human fibronectin (hFN, 100 ng/mL)-coated tissue culture flasks (BD Biosciences, East Rutherford, NJ, USA) and cultured with DMEM-F12 medium containing 10% v/v FBS, 1% v/v PenStrep, 2.5 ng/mL of TGF- β 1 (Peprotech, Rocky Hill, NJ, USA), and 5 ng/mL of PDGF- $\beta\beta$ (Peprotech). These cells, termed cBM-SMCs, were subsequently passaged when they attained near confluence and used further in our experiments. Phenotypic characterization of the differentiated cells was performed as described in our prior publication.^{15,19} To visualize the biodistribution of the cells in vivo, BM-MSCs and cBM-SMCs were labeled with either of the fluorescent probes, Vivo track 680TM (Perkin Elmer, Waltham, USA; to assess biodistribution at 24 h) or Luminicell Tracker 670 Cell Labeling Kit (EMD Millipore, Burlington, MA, USA; to assess biodistribution at 2 weeks) per the manufacturer's protocols. The labeled cell suspensions in each case were injected into anesthetized rats via the tail vein. Age- and weight-matched rats injected with vehicle (PBS) alone were assessed as the treatment controls. The timeline of experimental interventions and assessments is shown in [Supplementary Fig. S2](#).

Assessing In Vivo Biodistribution of Cells

At 24 h and 2 weeks after cell injection, the rats were euthanized by CO₂ asphyxiation. Major organs including the lungs, heart, aorta, liver, kidneys, and spleen were harvested. The organs were imaged with an IVIS Spectrum CT (Perkin Elmer, Waltham, MA, USA) with machine-defined settings

for the Vivo Track 680 ($\lambda = 675$ nm excitation, $\lambda = 720$ nm emission) and recommended settings for the Luminicell Tracker 670TM ($\lambda = 500$ -535 nm excitation, $\lambda = 660$ -680 nm emission). The sequence of images was then analyzed using Living Image Software (Perkin Elmer, Waltham, MA, USA). The corresponding organs of the cell-injected animal groups and treatment controls were imaged together and then analyzed. The total radiant efficiency of each set of organs was measured. Total radiant efficiency (TRE) is defined as the sum of fluorescence emission radiance per excitation power ($[\text{p/s}]/[\mu\text{W}/\text{cm}^2]$). The TRE values for the respective organs in treatment controls were averaged across replicate animals and then subtracted from the TRE value obtained for the corresponding organs for each cell-injected rat. This allowed us to obtain background-subtracted TRE values corresponding to the fluorescence signal emitted by the probe. The background-subtracted average TRE signals for 6 separate organs were plotted. For organs such as the kidneys, for which the TRE values in the cell-treated animals were lower than the background TRE values in the treatment control, the background-corrected values were negative. A 2-way ANOVA with Tukey multiple comparisons was performed to compare the statistical significance of differences in the background-subtracted TRE values between all the organs as well as 2 cell types separately for 24 h and 2 weeks.

Histology and Morphometric Analysis of Elastic Fibers in the AAA Tissue Sections

Histology and morphometric analysis of elastic fibers in the AAA tissue sections was done as per our previously published method.²⁰ The details have been described in [Supplementary methods 4](#).

Assessing Proteome Profile in the AAA Tissue Segment

The change in the proteome profile in the AAA tissue segment following cell injections was broadly assessed via a Proteome Profiler Array (R&D Systems, Minneapolis, MN, USA) per the manufacturer's instructions. Briefly, the AAA segment (section from renal bifurcation to the iliac bifurcation) from all the rats was harvested after euthanasia. Aortal segments from the same location, obtained from healthy, age-matched rats served as healthy controls. The aortal tissues were manually ground in liquid nitrogen and incubated in RIPA buffer for 20 min on ice, then homogenized by sonicating on ice. The samples were then centrifuged (14 000 g, 15 minutes, 4 °C). The supernatant containing protein was collected and the collected protein samples from 6 rats were pooled for each of the groups. Protein content in the pooled samples was quantified using a BCA protein assay kit (Thermo Fisher Scientific, Waltham, MA, USA). Cytokine array was detected using Proteome Profiler Rat XL Cytokine Array kit (R&D Systems, Minneapolis, MN, USA) as per manufacturer's instructions using the chemiluminescent method of detection. The blots were then imaged on a GE Amersham 600 Gel Imager (GE Healthcare, Chicago, IL, USA) in an auto exposure mode. The pixel density of each of the duplicate blots for each cytokine was measured with NIH ImageJ software. The average of duplicate values was plotted for each cytokine. Since we pooled the samples from 6 rats and performed the assay with $n = 1$ for each group, no statistical comparisons were performed.

Assessing Expression of Key Elastic Fiber Homeostasis Proteins and Proteins Regulating Tissue MMP Activity

Western blot analysis was used to assess changes in the expression of major elastin homeostasis proteins and upstream regulator proteins of MMP activity in the AAA wall with cell treatment at the 2-week time point. The segment of AAA wall tissue was isolated and processed as described in the section "Assessing Proteome Profile in the AAA Tissue Segment." The protein content in the aortal tissue isolated from each rat was measured using a Pierce BCA protein assay kit and a Western blot was performed.¹⁵ [Supplementary Table SI](#) lists the antibodies used to detect each of the proteins. Two-way ANOVA was used to compare the statistical significance of differences between the groups.

Statistical Analysis

All the statistical analysis was performed in Sigma Plot 13.0 (Systat Software Inc., San Jose, CA, USA). One-way or 2-way ANOVA was used to compare the statistical difference between the groups depending on the experiment as described

in the respective method section. The differences were deemed significant for $P < .05$ for all the experiments.

Results

Short- and Long-term Biodistribution of Cells In Vivo

The cell-associated fluorescence and the autofluorescence seen in each of the 6 organs for each of the cell-treated cases as well as treatment control are shown in [Fig. 1A](#). The biodistribution of cells as estimated from the total radiant efficiency corrected for tissue autofluorescence was analyzed. At 24 h, the distribution of cBM-SMCs between the organs was not different statistically. The fluorescence associated with the BM-MSCs was however significantly higher in the lungs versus all other organs ($P < .0001$) ([Fig. 1B](#)). Similarly, at the 24 h time point, the distribution of BM-MSCs was significantly higher than the distribution of cBM-SMCs in the lungs. At 2 weeks, the distribution of both cBM-SMCs and BM-MSCs was significantly higher in the lungs versus all other organs ([Fig. 1C](#)). However, no difference was seen between the 2 cell types in all the organs at 2 weeks.

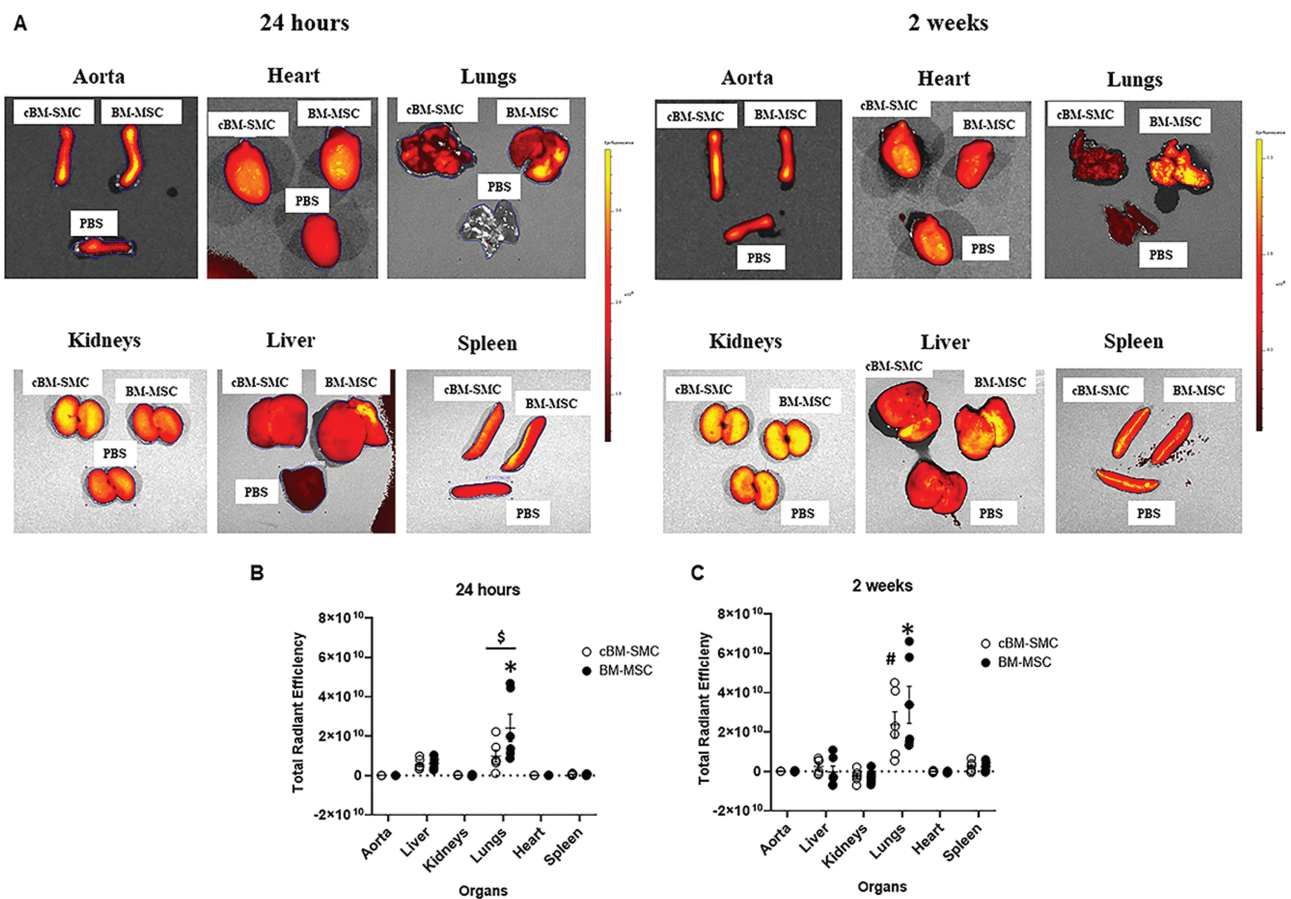


Figure 1. In vivo Biodistribution of Cells. **(A)** Ex-vivo images of organs taken using IVIS showing the distribution of cells in different organs at 24 h and 2 weeks. The fluorescence signal corresponds to the signals from cells labeled with cell tracker dyes. **(B)** Quantification of background subtracted fluorescence corresponding to both cBM-SMCs and BM-MSCs measured for each organ at 24 h. *represents significant difference of BM-MSCs for lungs versus all other organs and \$ represents significant difference between cBM-SMCs and BM-MSCs. **(C)** Quantification of background subtracted fluorescence corresponding to both cBM-SMCs and BM-MSCs measured for each organ at 2 weeks. Values shown are mean ± SD with individual data points represented by different scattered symbols for $n = 6$ animals/time point/case. *represents significant difference of BM-MSCs for lungs versus all other organs and # represents difference of cBM-SMCs for lungs versus all other organs deemed significant for $P < .05$ using a 2-way ANOVA with Tukey's multiple comparison.

Volumetric Assessment of Aorta using Phase-contrast Angiography (PCA) Magnetic Resonance Imaging

The results of the volumetric assessment of the aorta are described as follows:

(a) *Volume changes in the aorta with single-cell dosing event.*

The percentage change in volume of the aorta at baseline to AAA formation (B-AAA) versus aorta at baseline to 2 weeks after one dosing event of treatment (B-2W treatment) was not different for cBM-SMCs ($P = P_p = .075$) while B-AAA was significantly higher versus B-2W treatment for BM-MSC ($P = .005$) (Fig. 2A).

(b) *Volume changes in the aorta with 2 cell dosing events.*

The percentage change in volume of the aorta at baseline to AAA formation (B-AAA) versus aorta at baseline to 2 weeks after treatment with weekly dosing (B-2W treatment) was not different for all 3 groups (Fig. 2B).

(c) *Effect of a number of dosing events.* The percentage decrease in volume of the AAA segment of the aorta between baseline to 2 weeks after treatment (B-2W treatment) was significantly higher in the one dosing event versus the 2 dosing events for cBM-SMCs ($P = .014$). No such differences were seen between the one and 2 dosing events of BM-MSCs ($P = .137$) and the treatment controls ($P = .299$) (Fig. 2C).

(d) *Effect of time of cell treatment.* The percentage decrease in volume of the AAA segment between baseline and 2 weeks after treatment (B-2W treatment) was significantly higher versus the change between baseline and 1 week after treatment (B-1W treatment) for one dosing event of cBM-SMCs ($P = .019$) whereas no such difference was seen for one dosing event of BM-MSCs ($P = .069$) and treatment control ($P = .209$). However, B-1W treatment of BM-MSCs was significantly lower than the treatment control ($P = .048$) (Fig. 2D).

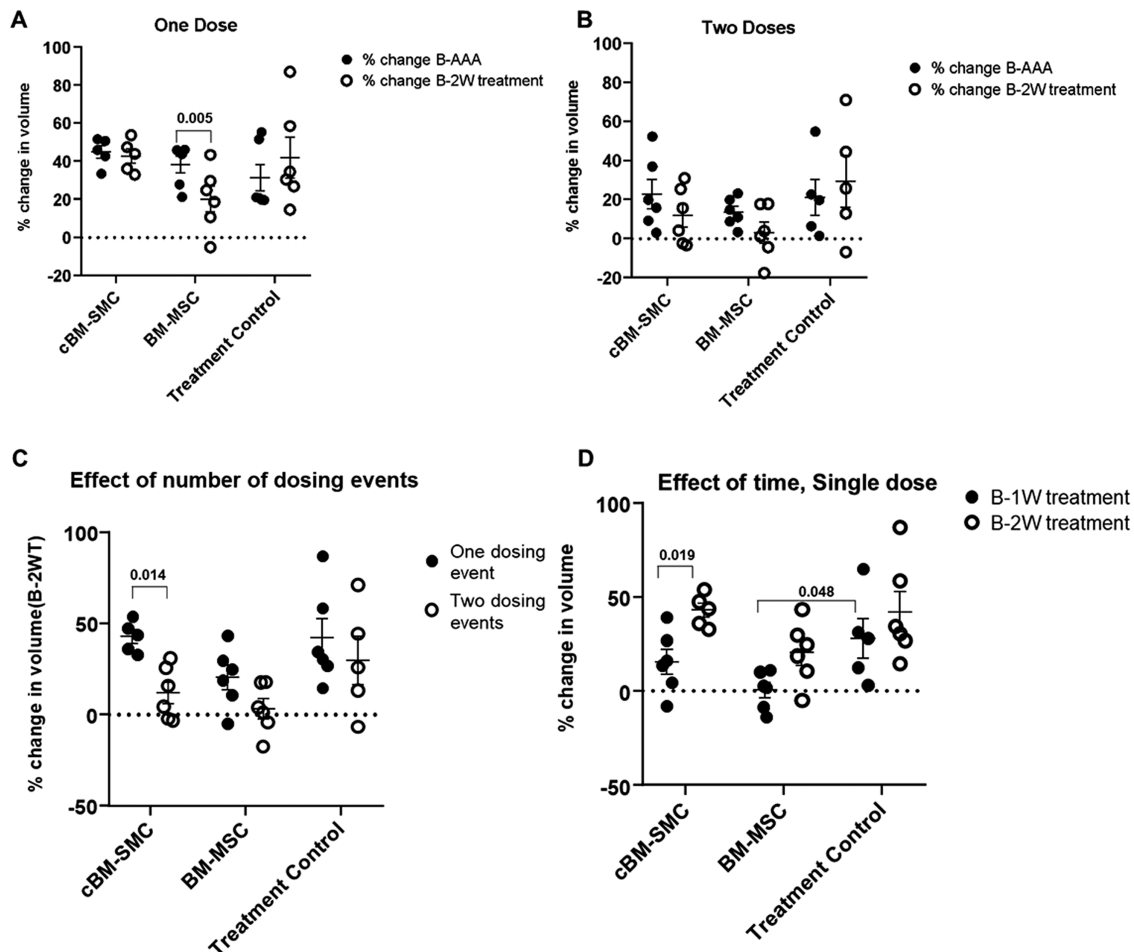


Figure 2. Quantitative volumetric assessment of aorta. (A) % change in the volume of aorta between baseline to AAA and baseline to 2 weeks after treatment for both cell types and treatment control after one dose of cell injection. (B) % change in the volume of aorta between baseline to AAA and baseline to 2 weeks after treatment for both cell types and treatment control after 2 doses of cell injection. (C) % change in the volume of aorta between baseline to 2 weeks after treatment for one and 2 dosing events showing the effect of number of dosing events on volume of AAA. (D) % change in the volume of aorta between baseline 1 weeks after treatment and baseline to 2 weeks after treatment for both cell types and treatment control showing the effect of time of treatment on volume of AAA. Values shown are mean \pm SD individual data points represented by scattered symbols for $n = 6$ animals/case deemed significant for $P < .05$. 2-way mixed model ANOVA was used to compare the statistical significance between the groups for each dose, and 2-way ANOVA was used to compare the effect of number of dosing events and effect of time between the groups and within the groups.

Morphometry of Elastic Matrix

Morphometric analysis of histological sections of the aorta showed a significantly higher total percent area of elastin in treatment control versus cBM-SMCs and BM-MSCs (Fig. 3A). However, no differences were seen between cBM-SMCs and BM-MSC-treated AAAs (Fig. 3A). Similarly, the mean of and variability in the area of objects identified as elastin was significantly higher in treatment control versus cBM-SMCs and BM-MSCs (Fig. 3E). The variability in perimeter length was significantly higher in treatment control versus cBM-SMCs and BM-MSCs (Fig. 3F) whereas tortuosity was not different between the groups (Fig. 3G), the

mean of and variability in maximum diameter was significantly higher in treatment control versus cBM-SMCs and BM-MSCs (Fig. 3D). Likewise, the mean minimum diameter which corresponds to the diameter of mature elastic fibers was significantly higher in treatment control versus cBM-SMCs whereas the variability in minimum diameter was significantly higher in treatment control versus both cBM-SMCs and BM-MSCs (Fig. 3E). The variability in perimeter length was significantly higher in treatment control versus cBM-SMCs and BM-MSCs (Fig. 3F) whereas tortuosity was not different between the groups (Fig. 3G).

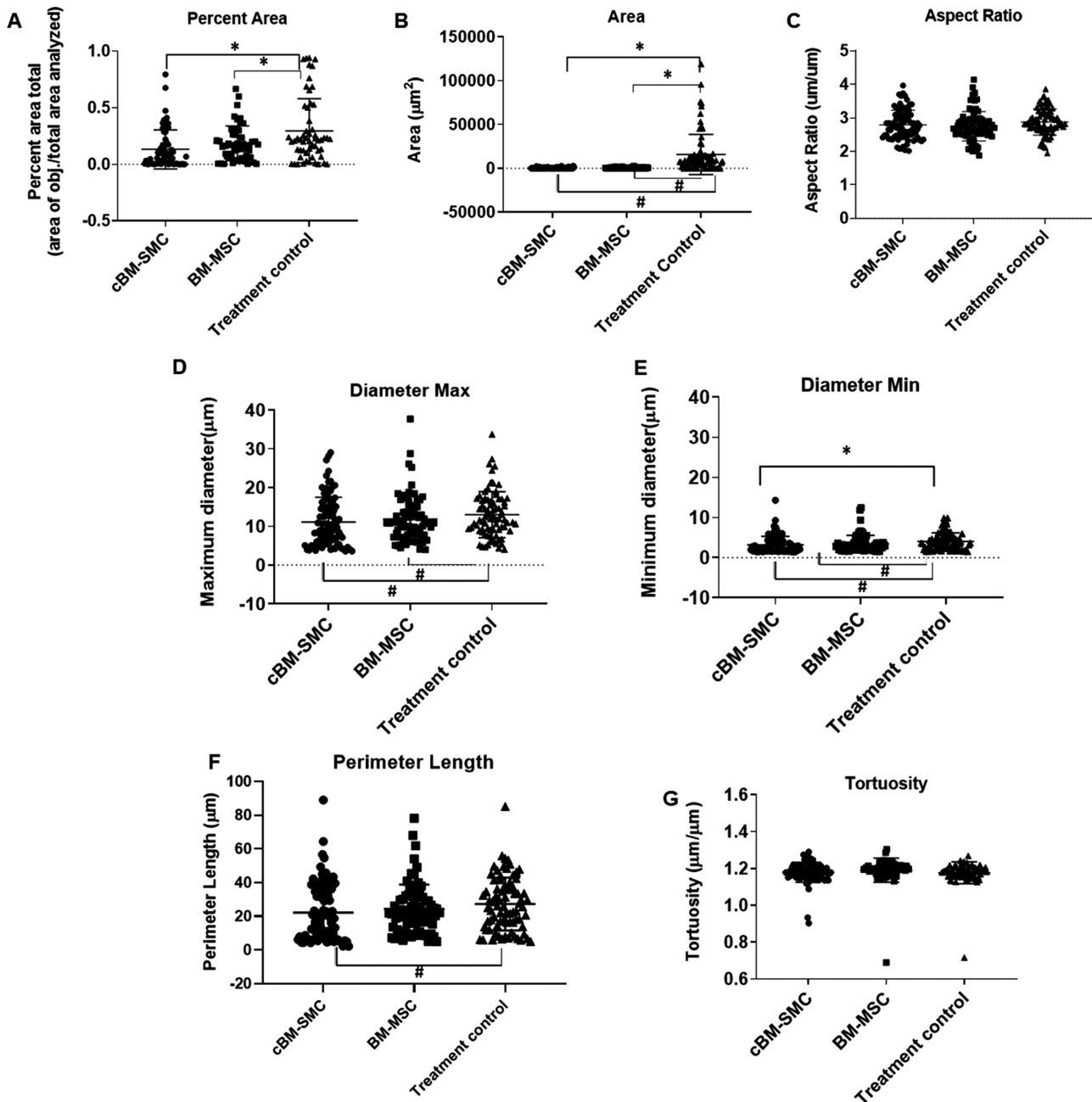


Figure 3. Quantitative morphometric analysis. Results of quantitative morphometric analysis of modified Hart stained tissue samples showing different parameters (A) percent area, (B) area, (C) aspect ratio, (D) diameter max, (E) diameter min, (F) perimeter length, (G) tortuosity. Values shown are mean \pm SD with individual data points represented by different scattered symbols. There were altogether 3 sections/animal and 6 animals/case, hence 18 total scattered symbols for each case. * indicates significance difference in mean and # represents significant difference in variability between the groups indicated by brackets deemed for $P < .05$ using one-way ANOVA.

Proteome Profiling using Cytokine Array

The directionality of the changes in cytokine expression relative to treatment controls is summarized in [Supplementary Table SII](#) and [Fig. 4](#). The proteome profile showed a reduction in the major inflammatory cytokines which are upregulated in AAA tissues including IFN- γ , IL-1 β , IL-3, IL-6, IL-17A, TNF- α , MMP-2, MMP-9, and MMP-3,²¹ with both one and 2 doses of cBM-SMCs compared to treatment controls. In BM-MSC-treated animals, IL-1 β , IL-3, IL-17A, and MMP-9 were reduced versus treatment controls, only in those rats that received 2 doses of cell inoculation. Lipocalin-2 which is known to enhance the activity of MMP-9,²² was also reduced upon cBM-SMCs

infusion (one and 2 dosing events), and BM-MSCs (2 dosing events only).

Elastin Homeostasis Protein and Upstream Regulator Proteins Expression in the Aorta Tissue Samples Using Western Blot

Total MMP-2 ([Fig. 5A](#)) and total TIMP-2 ([Fig. 5C](#)) expression normalized to treatment control were significantly lower in 2 dosing events versus one dosing event for both the cell types whereas total TIMP-1 ([Fig. 5B](#)) was significantly higher in the 2 dosing events versus one dosing event. No differences were seen between the cell types. Similarly, no difference was seen in the ratios of total MMP-2/total TIMP-2 ([Fig. 5D](#))

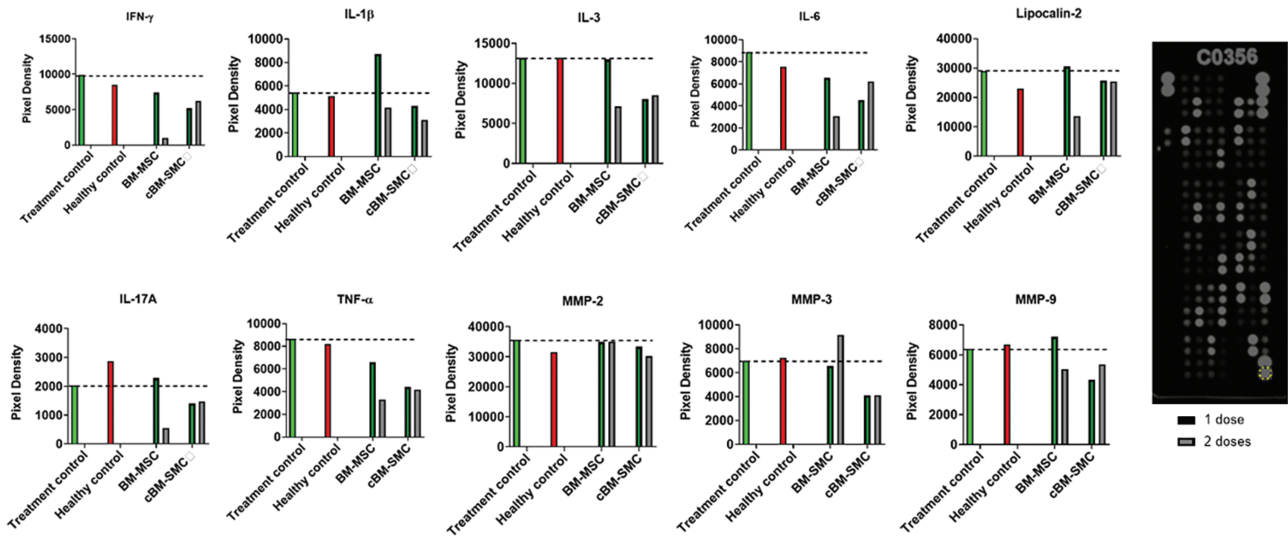


Figure 4. Cytokine array. Quantification of key inflammatory cytokines (in pixel density) implicated in AAAs using the cytokine array blot. The bars represent the means pixel density. The dotted line represents the level of cytokines in treatment control. The samples were pooled from 6 rats and assay was performed with $n = 1$ for each group. No statistical comparisons were performed.

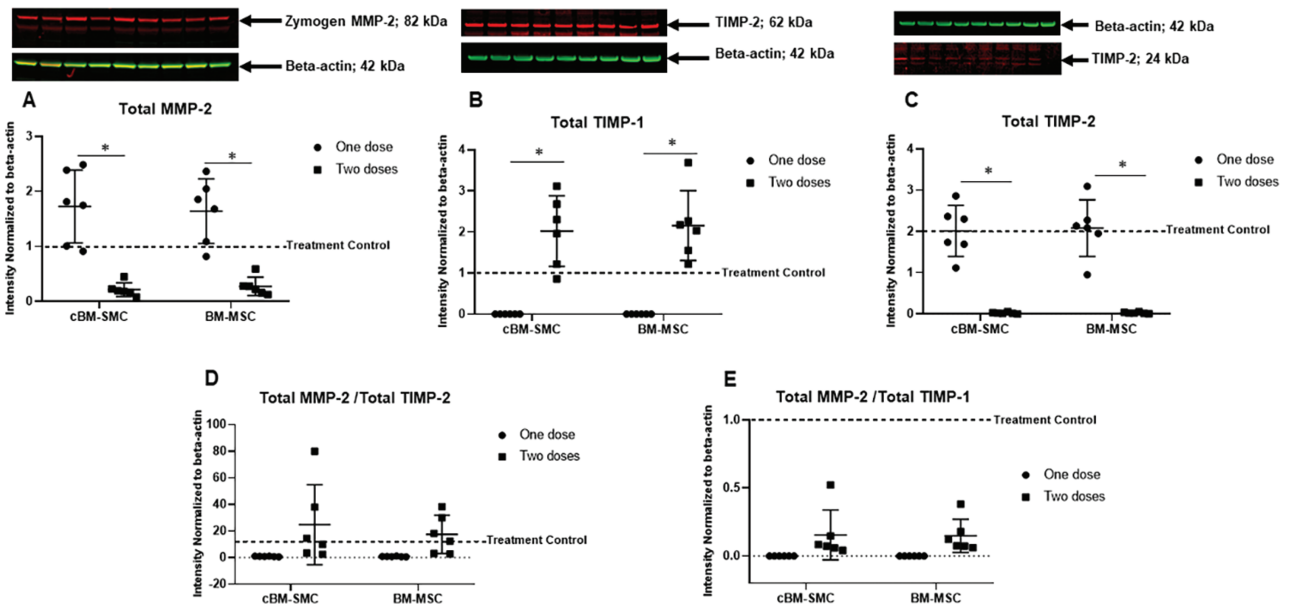


Figure 5. Western blot for MMPs and TIMPs. Quantification of Western blots performed on aorta tissue samples for **(A)** total MMP-2, **(B)** total TIMP-1, **(C)** total TIMP-2, **(D)** total MMP-2/total TIMP-2, and **(E)** total MMP-2/total TIMP-1. The bars represent mean \pm SD of protein samples collected from $n = 6$ animals/dose/case. The dotted line represents the treatment control and the values of proteins are normalized to treatment control. * represents significant difference between the groups indicated by bar deemed for $P < .05$ using a 2-way ANOVA.

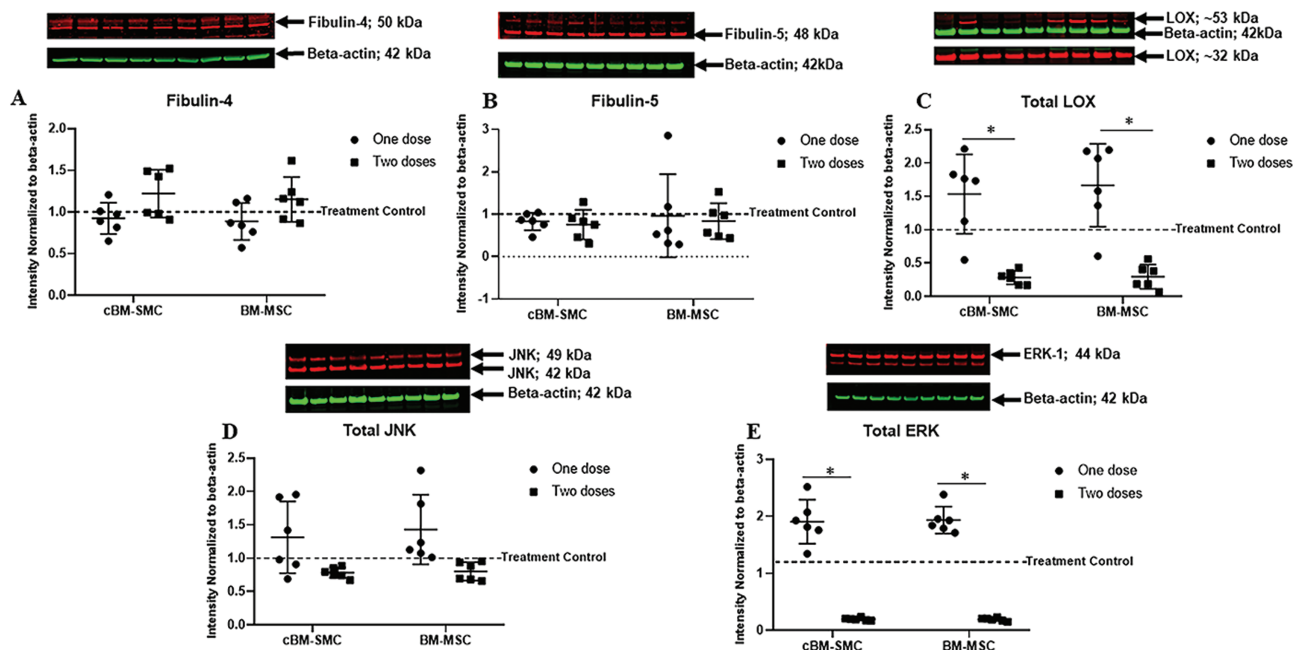


Figure 6. Western blots for elastin fiber homeostasis proteins and signaling proteins. Quantification of Western blots performed on aorta tissue samples for (A) Fibulin-4, (B) fibulin-5, (C) total LOX, (D) total JNK, and (E) total ERK. The bars represent mean \pm SD of protein samples collected from $n = 6$ animals/dose/case. The dotted line represents the treatment control and the values of proteins are normalized to treatment control. * represents significant difference between the groups indicated by bar deemed for $P < .05$ using a 2-way ANOVA.

and total MMP-2/total TIMP-1 (Fig. 5E) between the dosing events or the cell types. The expression of Fibulin-4 (Fig. 6A) and Fibulin-5 (Fig. 6B) was also not different between the dosing events as well as between the cell types. However, total LOX expression (Fig. 6C) was significantly higher in the one dosing event versus the 2 dosing events; again, no difference was seen between the cell types.

While we did not see any significant differences in the expression of total JNK (Fig. 6D) between the dosing events or between the cell types, the total ERK expression (Fig. 6E) was significantly lower in 2 dosing events versus one dosing event for both the cell types. No differences were noted between the cell types.

Discussion

Although our well-characterized MSC-derived SMCs (cBM-SMCs) exhibit high elastogenic capacity and are capable of providing anti-proteolytic and pro-elastogenic benefits to aneurysmal SMCs in vitro,^{14,15} the therapeutic benefits of MSCs and their derivatives can be influenced by several factors, which must be investigated for AAA treatment including (a) mode and invasiveness of cell delivery in vivo, (b) potential to home into the AAA wall and if at all necessary, for therapeutic action, (c) long-term engraftment and retention of the cells in target tissues, (d) ability to stimulate elastic matrix regenerative repair and attenuate inflammatory and proteolytic pathophysiology in the AAA wall toward slowing or reversing AAA growth, and (e) the differences between undifferentiated MSCs and their differentiated derivative cell phenotypes in their functional effects.²³ This work is designed as a first study to clarify these questions in the context of improving wall elastic matrix homeostasis for small AAA treatment.

We assessed the short-term (24 h) and long-term (2 weeks) bio-distribution of cells in organs in vivo upon one-time intravenous injection of a bolus of BM-MSCs and cBM-SMCs. The significant entrapment of BM-MSCs in the lungs versus all other organs at 24 h was not unexpected since entrapment of MSCs in the lung capillaries due to “pulmonary first pass effect” resulting from their larger size is well documented.²⁴ While the magnitude of the fluorescence signal associated with cBM-SMCs was higher in the lungs compared to other organs at 24 h, it was not deemed statistically significant (Fig. 1). This might be due to the smaller size of cBM-SMCs ($\sim 5 \mu\text{m}$) compared to BM-MSCs ($\sim 15\text{-}19 \mu\text{m}$) which allows most of the cBM-SMCs to bypass the pulmonary first-pass effect allowing them to localize in other organs as well. The fluorescence signal due to cBM-SMCs in the lungs was significantly lower compared to that of BM-MSCs at 24 h, which further supports our hypothesis that larger cell size contributes to the initial pulmonary entrapment of BM-MSCs, but not cBM-SMCs. Differently at 2 weeks both BM-MSCs and cBM-SMCs were significantly entrapped in the lungs. It is well-documented in literature that i.v.-administered MSCs are concentrated in the lung capillaries and are phagocytosed by monocytes within 24 h,²⁵ suggesting that the signal in the lungs detected at the 2-week time point may well be associated with phagocytes. This might also hold true in the case of cBM-SMCs which require further validation. Ruster et al. have also shown that P-selectin and a counter ligand expression by MSCs can contribute to their adhesion to the endothelium of the pulmonary vasculature and subsequent extravasation into the lung tissue.²⁶ While this might also be a possibility with our cBM-SMCs, which as BM-MSC derivatives, share many of their characteristics, further in-depth investigation is required to determine the factors that contribute to their localization in the lungs. The increasing trend of localization of both the cell types in the spleen at 2 weeks versus 24 h (Fig. 1A, 1B)

evokes published studies that have shown rapid interaction of transplanted stem cells with the cells of the immune system through circulating leukocytes or those in the skin, spleen and lymph nodes.²⁷ The entrapment of transplanted cells in the spleen is also suggested to be a potential mechanism of the immune suppressive effects of MSCs.²⁸ Indeed, studies have shown that shifts in the ratio of regulatory T cells to cytotoxic CD8+T-cells and also the polarization of TH1 cells to a cytokine profile-altered TH2 phenotype in splenocytes reduces antibody formation and T-cell responses against the transplanted allogeneic MSCs, hence failing to identify them.^{27,29} Some studies also suggest that entrapment of MSCs in the spleen and resulting T-cell responses are the potential route of MSC clearance.²⁷ However, the existence of physiological clearance pathways for transplanted MSCs still remains incompletely elucidated. The lack of activation of plasma C3 complement protein (Supplementary Fig. S3) relative to the treatment controls provides further corroboration that our injected cells do not trigger an immune response, although their ability to lower basal expression of the C3 complement to levels in healthy animals was not assessed.

Regardless of the rather limited localization of our injected cell types in the AAA wall, we proceeded to assess evidence of their therapeutic effect, motivated by recently published findings demonstrating their ability to act through paracrine mechanisms.³⁰ The volumetric assessment of aorta pre and post cell injection using MRI (Figs. 2 and 7) shows that while injection of a single dose of BM-MSCs caused an active, and significant volumetric reduction of the AAA segment, cBM-SMCs at least prevented an increase in segment volume, as seen in the treatment control animals. When the number of dosing events was increased (2 versus 1), we observed a trend of decreasing AAA segment volume although the mean difference was below the threshold for statistical significance, which is likely due to animal to animal variability and smaller sample size. A power analysis of our data predicts that with a sample size of 36 animals per group, the statistical significance will be evident. Differently, when comparing the effect of repeat dosing, 2 dosing events seem to be more effective for both cell types, which is also explained by the results of

the effect of time (2 weeks versus 1-week post-injection for a single-cell dosing event) which shows that without a repeat dose of cells 1 week after the first, the volume of aorta shows an increasing trend over the 2-week assessment period. The overall effect of changes in the volume of the aorta was also supported by the results of the cytokine array, which showed the decreasing trend of expression of a large number of documented inflammatory cytokines upon cell treatment (Fig. 4). Supplementary Table SII shows the directionality of change in AAA of various cytokines that were detected in the cell-treated AAA tissue samples and the implication of these changes to AAA progression, in light of their known function.

Besides the volumetric assessment of the aorta, we also evaluated the morphological changes in the elastic fiber structures as a function of cell injection using our earlier published morphometric technique applied to our Modified-Harts-stained histological sections.¹⁹ Analysis indicated larger elastin deposits in the treatment control as suggested by the significantly higher mean and variability of area (Fig. 3B). The size of these deposits (minimum diameter = 4.058 μm ; typical elastic fiber diameter ranges from 0.5 to 2.5 μm) suggests that they are larger clusters of elastin deposits and not fibers. The re-clustering of elastin into aggregates is a well-documented phenomenon that occurs during elastolysis.³¹ Thus, larger elastin deposits in the treatment controls but not in the cell-treated AAA tissues suggest that cell treatment is effective in controlling elastolysis. Moreover, the significantly higher variability of minimum and maximum diameter as well as perimeter length also suggests abnormal elastin homeostasis in the treatment control. The significantly higher percent area of the tissue sections occupied by the elastic matrix in the treatment control is likely due to the presence of a large number of disorganized elastin aggregates which further validates the hypothesis of continuous elastolytic activity in the treatment control, which is improved by cell delivery. While no difference was seen in the quantitative morphometric parameters between the 2 cell types, the presence of the large number of highly tortuous and continuous thick and mature fibers was observed in cBM-SMC-treated AAA tissues, which was similar to healthy control (Fig. 7)

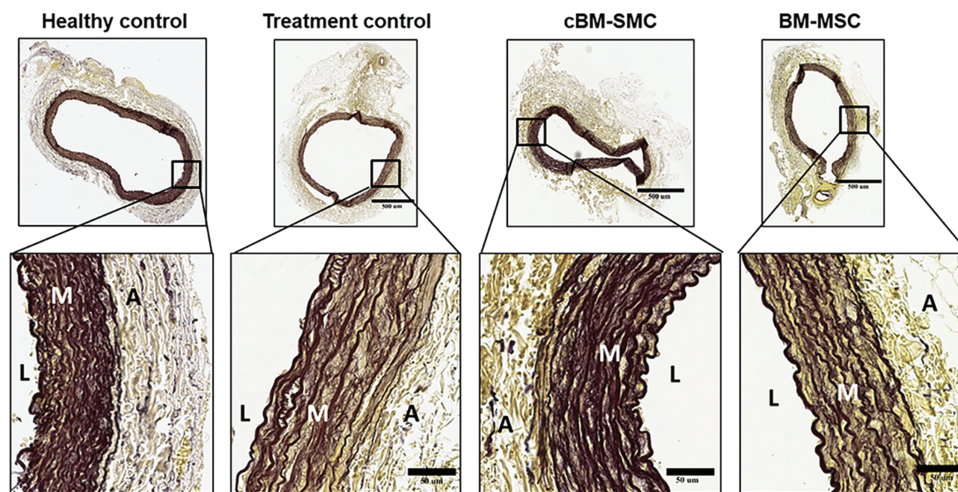


Figure 7. Sample histological images. Panel of modified Hart stained histological images showing whole tissue section of aorta (top row) and organization of elastic fibers (second row). Dark brown color represents elastic fibers and yellow color represents collagen and other tissue components. L, M, and A denotes lumen, media and, adventitia respectively. For color figure refer online version. Scale bar: 500 μm (top row) and 50 μm (bottom row).

whereas in BM-MSC-injected animals, fewer, and relatively thin elastic fibers were seen, and in treatment controls, only a few, thin, and clearly less tortuous elastic fibers were noted.

The outcomes of the morphometric analysis were further supported by the results of Western blot analysis. MMP2 is widely known to be implicated in elastic matrix breakdown in AAAs³¹ and the deficiency or downregulation of its natural inhibitors, the TIMPs 1 and 2 have been shown to be associated with AAA progression in both clinical and animal model scenarios.³¹ Our results shown in Fig. 5 suggest no significant effects of single dosing of either of the delivered cell types on MMP2 expression in the AAA wall, but significant reductions in the same upon repeat cell delivery, suggesting that the second dose of cells could have implications to reduced elastic matrix breakdown or conversely, to reducing impediments to neo-assembly and maintenance of new elastic fibers in the AAA wall. This is supported by our histological findings in Fig. 7. TIMP1 and TIMP2 analysis and calculated MMP-2/TIMP ratios for both TIMP types suggest that with 2 event cell dosing (both cell types), TIMP-1 appears to play a greater role in negative MMP-2 effects, leading to decreases in MMP-2/TIMP-1 ratios versus treatment controls indicative of net proteolytic activity (Fig. 5D, 5E). Such decreases were not noted following a single-cell-delivery event, at an identical 2-week post-intervention time. Again, the results support improved elastic matrix preservation and protected fiber assembly upon repeat cell dosing. No differences were noted in the anti-proteolytic effects of the 2 cell types.

The enzyme lysyl oxidase (LOX) is involved in crosslinking both collagen and elastic matrix in the aorta wall. While LOX increase suggests improved stabilization of elastic fibers, it can also suggest an enhanced and undesirable fibrotic response, typical in AAAs. Our data based on endpoint analysis of AAA wall tissue 2 weeks following initiating cell delivery suggests an upward trend in LOX expression with a single-cell dosing event, although the differences versus untreated controls were below the threshold for statistical significance; this has positive implications to stabilizing the elastic matrix. However, LOX levels measured at the same time point following 2-time cell dosing show a significant suppression, which needs further investigation. However, it is clear that such a decrease occurs only after the second dosing event, due to which elastic fiber stabilization can still benefit from effects due to the first cell inoculation. The process of the elastic fiber assembly process is a highly complex process with several dozen key proteins influencing various steps in hierarchical fiber assembly.³² A comprehensive spatiotemporal assessment of these proteins following stem cell/derivative delivery is mandated, which merits a separate follow-up study. However, an initial assessment of fibulins 4 and 5, 2 key elastic fiber assembly proteins,^{33,34} showed cell delivery to have no impact on their expression relative to treatment controls.

The upregulation of various proinflammatory cytokines including, but not limited to TNF- α , IL-1 β , IL-6, IL-3, IL-17A, MMPs, etc. are involved in the progression of AAAs²¹ (Supplementary Table SII) and most, if not all of these cytokines are known to activate JNK (c-Jun-N-terminal kinase), a mitogen-activated protein kinase (MAPK) also known as stress-activated protein kinase.²¹ Studies focused on the mechanistic aspect of AAA progression have shown inhibition of JNK to slow AAA growth.³⁵ The decreasing trend of JNK especially with 2 dosing events of cells in our study (Fig. 6) aligns with the outcome of cytokine array which

also shows the decreasing trend of inflammatory cytokines (Fig. 4) upon treatment with cells primarily the cBM-SMCs. Although the difference in JNK expression between the cell types or between the dosing events was not deemed significant statistically, likely due to the limited animal numbers per group, the trend shows that treatment with cBM-SMCs lowered JNK expression at both dosing events compared to BM-MSCs which again supports the outcome of histology and elastin homeostasis proteins expression (primarily MMPs and TIMPs) as described above. Similarly, another major MAPK signaling pathway involved in AAA progression is Extracellular Signal Related Kinase 1 and 2 (ERK 1 and 2). ERK1/2 is a critical modulator of MMPs which help in the recruitment of neutrophils and release cytokines at the site of inflammation.³¹ Our result shows that ERK expression was significantly reduced upon 2 dosing events of both cell types. Although no statistical difference was observed between the cell types, ERK expression of cBM-SMCs treated groups were lower than BM-MSCs treated groups. This result supports the outcome of reduced expression of MMP-2 and increased expression of TIMP-1 with repeat dosing. These outcomes indicate that cell therapy with stem cells, more so with the stem cells derivatives (cBM-SMCs), plays a significant role in regressing AAA by suppressing the MAPK signaling pathways primarily JNK and ERK which in turn restores the tissue homeostasis by reducing proteolytic activity. However, a more rigorous pre-clinical study is mandated to confirm these outcomes with statistical significance for the results which have shown a positive trend.

Overall, our results suggest that cBM-SMCs retain in the AAA site for a longer time period compared to BM-MSCs, cell treatment potentially attenuates overall inflammation, enhances new elastic fiber formation, and improves elastic fiber stability through anti-proteolytic effects, outcomes that are more pronounced with repeat cell treatments and with the delivery of BM-MSC-derived cBM-SMCs.

Funding

This study was supported by grants from the National Institutes of Health (HL139662) awarded to Anand Ramamurthi and a pre-doctoral fellowship from the American Heart Association (19PRE34390083).

Conflict of Interest

The authors declared no potential conflicts of interest.

Author Contributions

S.Dahal: conception and design, collection and/or assembly of data, data analysis and interpretation, manuscript writing. S.Dayal: collection and assembly of data, data analysis and interpretation, manuscript writing. C.A.: collection and assembly of data, data analysis and interpretation. J.P.: collection and assembly of data. A.R.: conception and design, financial support, assembly of data, data analysis and interpretation, manuscript writing, final approval of manuscript.

Data Availability

The data that support the findings of this study are available from the corresponding author upon reasonable request.

Supplementary Material

Supplementary material is available at *Stem Cells Translational Medicine* online

References

- Kolios G, Moodley Y. Introduction to stem cells and regenerative medicine. *Respiration*. 2012;85:3-10.
- Kumar D, Chandra B. Regenerative medicine: recent advances and potential applications. *J Biosci Bioeng Biotechnol*. 2016;03:1-5.
- De Becker A, Van Riet I. Homing and migration of mesenchymal stromal cells: how to improve the efficacy of cell therapy? *World J Stem Cells*. 2016;8:73-87.
- Gnecchi M, Zhang Z, Ni A, Dzau VJ. Paracrine mechanisms in adult stem cell signaling and therapy. *Circ Res*. [Internet]. 2008;103:1204-19. doi:10.1161/CIRCRESAHA.108.176826
- Gnecchi M, Danieli P, Malpasso G, Ciuffreda MC. Paracrine mechanisms of mesenchymal stem cells in tissue repair. *Methods Mol Biol*. [Internet]. 2016;1416:123-46. doi:10.1007/978-1-4939-3584-0_7
- Mirotsoy M, Jayawardena TM, Schmeckpeper J, Gnecchi M, Dzau VJ. Paracrine mechanisms of stem cell reparative and regenerative actions in the heart. *J Mol Cell Cardiol*. 2011;50:280-289. doi:10.1016/j.yjmcc.2010.08.005
- Yamawaki-Ogata A, Hashizume R, Fu X-M, Usui A, Narita Y. Mesenchymal stem cells for treatment of aortic aneurysms. *World J Stem Cells*. [Internet]. 2014;6:278-87. doi:10.4252/wjsc.v6.i3.278
- Midha S, Jain KG, Bhaskar N, et al. Tissue-specific mesenchymal stem cell-dependent osteogenesis in highly porous chitosan-based bone analogs. *Stem Cells Transl Med*. 2021;10:303-319.
- Aggarwal S, Qamar A, Sharma V, Sharma A. Abdominal aortic aneurysm: a comprehensive review. *Exp Clin Cardiol*. 2011;16:11-15.
- Thompson RW, Geraghty PJ, Lee JK. Abdominal aortic aneurysms: basic mechanisms and clinical implications. *Curr Probl Surg*. 2002;39:110-230. doi:10.1067/msg.2002.121421
- Wang G, Jacquet L, Karamariti E, Xu Q. Origin and differentiation of vascular smooth muscle cells. *J Physiol*. 2015;593:3013-3030. doi:10.1113/jp270033
- Descamps B, Emanuelli C. Vascular differentiation from embryonic stem cells: novel technologies and therapeutic promises. *Vascul Pharmacol*. [Internet]. 2012;56:267-79. doi:10.1016/j.vph.2012.03.007
- Dash BC, Jiang Z, Suh C, Qyang Y. Induced pluripotent stem cell-derived vascular smooth muscle cells: methods and application. *Biochem J*. 2015;465:185-194. doi:10.1042/BJ20141078
- Doetschman T, Shull M, Kier A, Coffin JD. Embryonic stem cell model systems for vascular morphogenesis and cardiac disorders. *Hypertension*. [Internet]. 1993;22:618-29. doi:10.1161/01.hyp.22.4.618
- Dahal S, Broekelman T, Mecham RP, Ramamurthi A. Maintaining elastogenicity of mesenchymal stem cell-derived smooth muscle cells in two-dimensional culture. *Tissue Eng—Part A*. 2018;24:979-989.
- Dahal S, Swaminathan G, Carney S, et al. Pro-elastogenic effects of mesenchymal stem cell derived smooth muscle cells in a 3D collagenous milieu. *Acta Biomater*. 2020;105: 180-190.
- Swaminathan G, Stoilov I, Broekelmann T, Mecham R, Ramamurthi A. Phenotype-based selection of bone marrow mesenchymal stem cell-derived smooth muscle cells for elastic matrix regenerative repair in abdominal aortic aneurysms. *J Tissue Eng Regen Med*. [Internet]. 2016;12:e60-e70 [cited 2017 Apr 13].
- Gacchina CE, Deb P, Barth JL, Ramamurthi A. Elastogenic inductability of smooth muscle cells from a rat model of late stage abdominal aortic aneurysms. *Tissue Eng Part A*. [Internet]. 2011;17:1699-711. doi:10.1089/ten.TEA.2010.0526
- Swaminathan G, Gadepalli VS, Stoilov I, et al. Pro-elastogenic effects of bone marrow mesenchymal stem cell-derived smooth muscle cells on cultured aneurysmal smooth muscle cells. *J Tissue Eng Regen Med*. 2017;11:679-693.
- Dahal S, Kuang M, Rietsch A, et al. Quantitative morphometry of elastic fibers in pelvic organ prolapse. *Ann Biomed Eng*. 2021;49:1909-1922.
- Middleton RK, Lloyd GM, Bown MJ, et al. The pro-inflammatory and chemotactic cytokine microenvironment of the abdominal aortic aneurysm wall: a protein array study. *J Vasc Surg*. 2007;45:574-580. doi:10.1016/j.jvs.2006.11.020
- Kobara H, Miyamoto T, Suzuki A, et al. Lipocalin2 enhances the matrix metalloproteinase-9 activity and invasion of extravillous trophoblasts under hypoxia. *Placenta*. 2013;34:1036-1043. doi:10.1016/j.placenta.2013.08.004
- Choumerianou DM, Dimitriou H, Kalmanti M. Stem cells: promises versus limitations. *Tissue Eng Part B Rev*. [Internet]. 2008;14:53-60. doi:10.1089/teb.2007.0216
- Fischer UM, Harting MT, Jimenez F, et al. Pulmonary passage is a major obstacle for intravenous stem cell delivery: the pulmonary first-pass effect. *Stem Cells Dev*. 2009;18:683-692.
- Gonçalves FDC, Luk F, Korevaar SS, et al. Membrane particles generated from mesenchymal stromal cells modulate immune responses by selective targeting of pro-inflammatory monocytes. *Sci Rep*. 2017;7:1-13.
- Rüster B, Göttig S, Ludwig RJ, et al. Mesenchymal stem cells display coordinated rolling and adhesion behavior on endothelial cells. *Blood*. 2006;108:3938-3944. doi:10.1182/blood-2006-05-025098
- Leibacher J, Henschler R. Biodistribution, migration and homing of systemically applied mesenchymal stem/stromal cells. *Stem Cell Res Ther*. [Internet]. 2016;7:7. doi:10.1186/s13287-015-0271-2
- Weiss ARR, Dahlke MH. Immunomodulation by Mesenchymal Stem Cells (MSCs): Mechanisms of action of living, apoptotic, and dead MSCs. *Front Immunol*. 2019;10:1-10.
- Kurtz A. Mesenchymal stem cell delivery routes and fate. *Int J Stem Cells*. [Internet]. 2008;1:1-7. doi:10.15283/ijsc.2008.1.1.1
- Liang X, Ding Y, Zhang Y, Tse HF, Lian Q. Paracrine mechanisms of mesenchymal stem cell-based therapy: current status and perspectives. *Cell Transplant*. 2014;23:1045-1059. doi:10.37270/96368913X667709
- Zhong J, Gencay MMC, Bubendorf L, et al. ERK1/2 and p38 MAP kinase control MMP-2, MT1-MMP, and TIMP action and affect cell migration: a comparison between mesothelioma and mesothelial cells. *J Cell Physiol*. 2006;207:540-552.
- Hiromi Y, Davis EC. Unraveling the mechanism of elastic fiber assembly: the roles of short fibulins. *Int J Biochem Cell Biol*. 2010;42:1084-1093.
- Choudhury R, McGovern A, Ridley C, et al. Differential regulation of elastic fiber formation by fibulin-4 and -5. *J Biol Chem*. 2009;284:24553-24567. doi:10.1074/jbc.M109.019364
- Yamauchi Y, Tsuruga E, Nakashima K, Sawa Y, Ishikawa H. Fibulin-4 and -5, but not fibulin-2, are associated with tropoelastin deposition in elastin-producing cell culture. *Acta Histochem Cytochem*. 2010;43:131-138.
- Yoshimura K, Aoki H, Ikeda Y, et al. Regression of abdominal aortic aneurysm by inhibition of c-Jun N-terminal kinase. *Nat Med*. 2005;11:1330-1338.